Epstein–Barr virus reactivation induces MYC-IGH spatial proximity and t(8;14) in B cells

Fatimata Bintou Sall, Anna Shmakova, Anna Karpukhina, Tatyana Tsfasman, Nikolai Lomov, Reynand Jay Canoy, David Boutboul, Eric Oksenhendler, Awa Oumar Toure, Marc Lipinski, et al.

Epstein-Barr Virus reactivation induces *MYC-IGH* spatial proximity and t(8;14) in B cells

Shortened title: EBV reactivation, *MYC-IGH* proximity and t(8;14)

Fatimata Bintou Sall[1,2], Anna Shmakova[1,3,4], Anna Karpukhina[1,4], Tatyana Tsfasman[1], Nikolai Lomov[1,5], Reynand Canoy[1], David Boutboul[6], Eric Oksenhendler[6], Awa Oumar Toure[2], Marc Lipinski[1], Joëlle Wiels[1], Diego Germini[1,7], Yegor Vassetzky[1,4,7]

[1]UMR9018, Université Paris-Saclay, CNRS, Gustave Roussy, Villejuif, France
[2]Faculty of Medicine, Pharmacy and Odontology, Cheikh Anta Diop University of Dakar, Senegal
[3]Laboratory of Molecular Endocrinology, Institute of Experimental Cardiology, Federal State Budgetary Organization National Cardiology Research Center Ministry of Health of the Russian Federation, Moscow, Russia
[4]Koltzov Institute of Developmental Biology, Russian Academy of Sciences, Moscow, Russia
[5]Faculty of Biology, State University of Moscow, Russia
[6] Service d'Immunopathologie Clinique, Hôpital St Louis, APHP, 75012 Paris, France.
[7]Corresponding authors:
yegor.vassetzky@cnrs.fr
germinidiego@gmail.com

Keywords

EBV; Burkitt Lymphoma, lymphomagenesis; t(8;14); CRISPR/Cas9; MRE11.

Contact information:

Fatimata Bintou Sall fabisall3007@gmail.com
Anna Shmakova anyashm@gmail.com
Anna Karpukhina anna.karpukhina12@gmail.com
Tatyana Tsfasman tanya.tsfasman@gmail.com
Nikolai Lomov lomov13@gmail.com
Reynand Canoy rccanoy@up.edu.ph
David Boutboul david.boutboul@aphp.fr
Eric Oksenhendler eric.oksenhendler@aphp.fr
Awa Oumar Toure awaoumar2000@yahoo.fr
Marc Lipinski Marc.LIPINSKI@gustaveroussy.fr
Joëlle Wiels Joelle.WIELS@gustaveroussy.fr
Diego Germini germinidiego@gmail.com
Yegor Vassetzky yegor.vassetzky@cnrs.fr

Corresponding authors:
Yegor Vassetzky, Ph.D.
Directeur de Recherche CNRS
Chromatin Dynamics and Metabolism in Cancer

CNRS UMR9018
Institut Gustave Roussy
39, rue Camille-Desmoulins
94805 Villejuif, France
Tel: +33(0)1 42 11 62 83
Fax: +33(0)1 42 11 54 94
http://umr9018.cnrs.fr/la-recherche/equipe3/
Email: yegor.vassetzky@cnrs.fr

Diego Germini, Ph.D.
CNRS UMR9018
Institut Gustave Roussy
39, rue Camille-Desmoulins
94805 Villejuif, France
Tel: +33(0)1 42 11 62 83
Fax: +33(0)1 42 11 54 94
http://umr9018.cnrs.fr/la-recherche/equipe3/
Email: germinidiego@gmail.com

Data availability statement
All data generated or analysed during this study are included in this published article and its additional files. No unique code or sequencing data was generated during the study. A semi-automatic macro for ImageJ is available at https://github.com/AnnaK135/sall2021_bmrf1.git.

Funding
This study was supported by grants from the INSERM (ENVIBURKITT), La Ligue Contre le Cancer (M27231) and the IDB RAS government basic research program 0088-2021-0007. FBS was a recipient of the grants from the Institut Servier and Service de coopération et d'action culturelle de l'Ambassade de France au Sénégal. AK is a recipient of the Eiffel Fellowship from Campus France. This study was supported by a grant from TA2019 and TA2021, Univ. Paris Sud, université Paris Saclay, France.

Conflict of interests disclosure
The authors declare that there is no conflict of interest

Ethics approval statement
Three patients were included in the study after obtaining an informed consent and a review by the local ethic committee (IMMUNOLYMPH protocol, CLEA-2020-113).

Patient consent statement
Three patients were included in the study after obtaining an informed consent and a review by the local ethic committee (IMMUNOLYMPH protocol, CLEA-2020-113).

Permission to reproduce material from other sources
Not applicable

Clinical trial registration
Not applicable

Text word count: 4809
Abstract word count: 147
Statement of significance word count: 52
The number of figures: 5
The number of tables: 1
The number of Supplementary Figures: 7
The number of Supplementary Tables: 3 supplementary
The number of references: 77

Abstract

Burkitt lymphoma (BL) is a B cell malignancy associated with the Epstein-Barr virus (EBV). Most BL cases are characterized by a t(8;14) chromosomal translocation involving the *MYC* oncogene and the immunoglobulin heavy chain gene (*IGH*). The role of EBV in promoting this translocation remains largely unknown. Here we provide the experimental evidence that EBV reactivation from latency leads to an increase in the proximity between the *MYC* and *IGH* loci, otherwise located far away in the nuclear space both in B-lymphoblastoid cell lines and in patients' B-cells. Specific DNA damage within the *MYC* locus, followed by the MRE11-dependent DNA repair plays a role in this process. Using a CRISPR/Cas9-based B cell model to induce specific DNA double strand breaks in *MYC* and *IGH* loci, we have shown that the *MYC-IGH* proximity induced by EBV reactivation leads to an increased t(8;14) translocation frequency.

Statement of significance

This study analysed the role of EBV reactivation in the occurrence of Burkitt lymphoma-specific t(8;14) chromosomal translocations. Our findings demonstrate that EBV reactivation induces MRE11-dependent proximity between the *MYC* and *IGH* loci in B cells, which translates into elevated t(8;14) rates upon induction of DSBs within these loci.

Graphical abstract

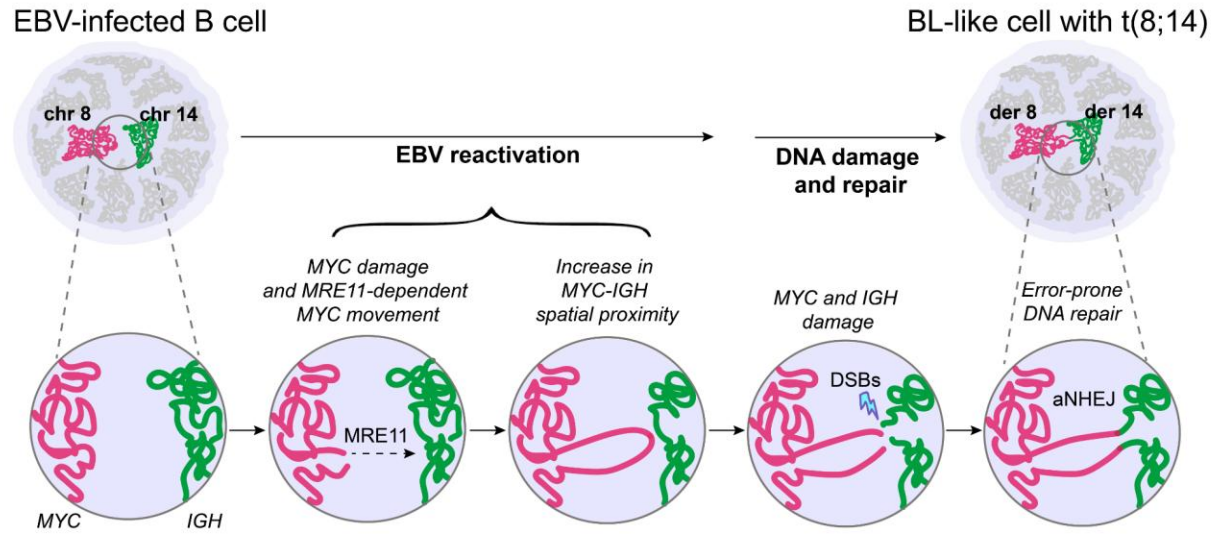

Introduction

Burkitt lymphoma (BL) is an extremely aggressive non-Hodgkin B cell malignancy with a geographically variable incidence and features. In Europe and US, BL is sporadic or associated with human immunodeficiency virus (HIV), while in African regions, it's endemic and nearly always associated with Epstein-Barr virus (EBV)(1–4).

EBV, the first described human oncovirus, is a □-herpesvirus infecting mainly B lymphocytes. Its life cycle is composed of two distinct phases: the lytic phase when viral particles are produced and the latent phase when the viral genome persists as an extrachromosomal episome in the host cell nucleus (5–8). The switch from latency to lytic cycle is mainly triggered by the *BZLF1* and *BRLF1* genes encoding for the transcriptional activators Zebra (or Zta) and Rta, respectively. Both are expressed at the onset of the lytic cycle and are often used as markers of lytic cycle activation (9–12). The complete lytic cycle involves viral genome replication, infected cell lysis and release of new infectious virions while an abortive lytic cycle is characterized by the expression of immediate early and early lytic proteins without genome replication or cell lysis(13). EBV replication rarely leads to cell lysis and the virus is secreted from live cells, through the secretory pathway(14). Moreover, only a minority of EBV-infected memory B cells from healthy carriers complete a productive lytic cycle after stimulation(13). EBV-associated diseases display various types of EBV latency but there is a growing number of reports showing that the lytic phase, both complete and abortive, could contribute to the process of oncogenesis (reviewed in(10,15)).

BL cells always display chromosomal translocations involving the *MYC* oncogene on chromosome 8 and one of the genes coding for the immunoglobulin heavy (*IGH*) or light chains (*IGK* or *IGL*) on chromosomes 14, 2 and 22, respectively; the t(8;14) translocation is found in more than 80% of cases(16–19). So far, specific mechanisms leading to the t(8;14) translocation in BL remain largely unknown.

To be generated, a translocation requires simultaneous DNA double strand breaks (DSBs) on the two partner chromosomes, DSB repair through the error-prone non-homologous end-joining (NHEJ) pathway and the spatial proximity between the two partners (20–22). EBV, in both its life cycle phases, can interact with chromatin remodelling complexes or lead to epigenetic alterations, DNA damage and, consequently, to B cell nuclear remodelling (reviewed in(23)). These effects can predispose to chromosomal translocations. Nevertheless, there is still no direct evidence for EBV implication in the BL t(8;14) translocation.

Here, we investigated the role of EBV in t(8;14) generation. Modelling the role of EBV in the BL is challenging, since the translocation formation results from the combination of very rare events in B cells: DSBs formation at *MYC* and *IGH* loci, their proximity and erroneous repair. Moreover, only a minority of primary B cells from blood are EBV positive (1-50 out of 10^6 during latency(24)). That is why we used an experimental system for specific induction of t(8;14) in EBV-transformed B cells, and we provided the first direct evidence that EBV reactivation led to an increased rate of the *MYC-IGH* colocalization which promoted a higher rate of the t(8;14). This newly acquired *MYC-IGH* proximity was triggered by a specific DNA damage at *MYC* locus and driven by the subsequent MRE11-dependent DNA repair. Our findings were confirmed *in vivo* in B-cells of patients with EBV-related lymphoproliferative disorders.

Results

1. EBV reactivation leads to *MYC-IGH* colocalization in lymphoblastoid cell lines

Chromosomal translocations are induced by the NHEJ, a proximity-based mechanism(25), but in human naive B cells, *MYC* and *IGH* loci are separated in the nuclear space(26,27). As EBV infection and reactivation are accompanied by large-scale modifications in the nuclear architecture(28–30), we hypothesised that this could affect the nuclear localization of the *MYC* and *IGH* loci.

To study the effect of EBV reactivation on *MYC* and *IGH* spatial localization within the nuclear space, we first determined the optimal virus reactivation conditions in RPMI8866 and PRIESS lymphoblastoid cell lines (LCLs) (see Supplementary Fig. 1). We observed a high level of virus reactivation in RPMI8866 cells treated with sodium butyrate (NaB) or Zebra protein (Supplementary Fig. 1a,b,f). Thus, for the following experiments, we used Zebra protein and NaB to induce the lytic cycle in RPMI8866 cells.

We next analysed the localization of the *MYC* and *IGH* loci in the tridimensional nuclear space of primary B cells, RPMI8866 and PRIESS cell lines (treated or not with EBV lytic cycle inducers) using 3D-fluorescence *in situ* hybridization (FISH). *MYC* and *IGH* loci were considered as colocalized when the centres of their fluorescent foci were 1 µm or less from each other (Fig 1a). In naive B cells from healthy donors, *MYC* and *IGH* loci were colocalized in 5.80%±0.57 cells (n=180 cells); in latent non-treated RPMI8866 and PRIESS cells, *MYC* and *IGH* loci colocalization was also low (4.55%±0.88 and 2.78%±0.78, respectively; n≥100 cells; Fig. 1a and Supplementary Fig. 1d). EBV lytic cycle induction in RPMI8866 cells increased the *MYC-IGH* colocalization twofold (8.7%±0.56 in NaB treated cells and 9.52%±0.25 in Zebra-treated cells vs 4.55%±0.88 in latent RPMI8866 cells; $p<0.001$; n≥100 cells; Fig. 1a,b). Lytic cycle activation in PRIESS cells also increased twofold the colocalization between the *MYC* and *IGH* loci (Supplementary Fig. 1d). Thus, EBV reactivation led to a significant increase in *MYC-IGH* colocalization rate in LCLs. Importantly, EBV reactivation did not cause cell cycle arrest in our model (Supplementary Fig. 2a,b).

We next tested whether the *MYC-IGH* colocalization observed upon EBV reactivation could be directly induced by the Zebra protein. Indeed, Zebra interacts with host genes and may thus affect their expression and, consequently, spatial localization (reviewed in(10)). We treated B lymphocytes from healthy donors with the recombinant Zebra protein for various times. Zebra was detectable in B cells 6h after treatment, peaked at 24h and remained in the cells at 48h (Fig. 1c). No difference in *MYC-IGH* colocalization rate was detected in Zebra-treated naive or activated B cells as compared to the untreated controls (Fig. 1d,e). *Z*ebra treatment did not affect B cell cycle (Supplementary Fig. 2c). The increase in *MYC-IGH* colocalization rate in activated B cells relative to non-activated B cells is consistent with previous reports(31). Zebra alone is therefore not sufficient to induce *MYC-IGH* proximity in EBV-negative B cells.

2. LCLs with spontaneous EBV lytic cycle show an increased spatial proximity between the *MYC* and *IGH* loci

To confirm that EBV lytic cycle affects the proximity of the *MYC* and *IGH* loci, we used two additional LCLs, M81 and rMSHJ, with a high spontaneous lytic activity (32,33). Their spontaneous lytic activity was confirmed by expression of EBV immediate early (*BZLF1* and *BRLF1)* and late (*BDRF1* and *BLLF1*) genes and BMRF1 protein (Fig. 1f,g; Supplementary Fig. 1e,g;3a,b).

Both M81 and rMSHJ cells presented a significantly higher *MYC-IGH* colocalization rate than non-stimulated RPMI8866 (14.98%±1.59 in M81 cells and 15.54%±1.77 in rMSHJ cells vs 4.56%±0.62 in RPMI8866; $p<0.05$; n≥200 cells Fig. 1h). Moreover, using immunofluorescent staining for EBV early protein BMRF1 (whose transcription is activated by the Zebra) in M81 cells, we found that *MYC-IGH* colocalization was significantly higher in BMRF1-positive cells as compared to BMRF1-negative ones (43.89±3.70 vs 7.77%±3.30, $p<0.0001$; OR 6.376 [2.396-15.96], $\chi^2=16.79$, $p<0.0001$; n≥60 cells, Fig. 1i,j). These results reinforce our conclusion that EBV reactivation induces the proximity between the *MYC* and *IGH* loci in the nuclear space.

3. B cells from individuals with EBV-related lymphoproliferative disorders and immune suppression present an increased spatial proximity between the *MYC* and *IGH* loci

We next assessed the proximity of the *MYC* and *IGH* loci in B cells from three patients (P1-P3) with EBV-related lymphoproliferative disorders (Table 1). Case history can be found in the Supplementary Materials. B cells from P1 and P2 with EBV-related lymphoproliferative disorders and immune suppression had a significantly elevated *MYC-IGH* colocalization rate compared to B cells isolated from healthy donors (Table 1). A trend to increased *MYC-IGH* colocalization rate was observed in P3 with a severe infectious mononucleosis, although very few circulating B cells in P3 blood did not allow larger sampling to obtain statistical significance.

To confirm that *MYC-IGH* colocalization can be driven by EBV reactivation, we focused on a unique case of primary EBV infection on the background of immune suppression caused by kidney transplant from EBV+ donor into an EBV- recipient (P1). PBMCs obtained from P1 were spontaneously transformed in culture (Supplementary Fig. 4). As mentioned above, B cells from P1 presented a significantly higher *MYC-IGH* colocalization rate than B cells from healthy donors (Table 1). Moreover, EBV-infected B cells were undergoing a lytic cycle as observed by BMRF1 staining (Fig. 2a). We found that *MYC-IGH* colocalization was significantly higher in BMRF1-positive cells as compared to all B cells from P1 (34.60%±2.203 vs 21.46%±2.363; n≥50 cells; $p<0.01$; Fig. 2b,2c). These results demonstrate that EBV reactivation is associated with the increased proximity between the *MYC* and *IGH* loci *in vivo*.

4. Development and characterization of the MYCIGHC9 cell line to induce and detect the *MYC-IGH* translocation

In B cells from healthy individuals, spontaneous translocations are exceedingly rare, occurring in approximately $1x10^{-6}$ cells(34), and thus undetectable by standard cytogenetic techniques. In addition, endemic BL translocations occur over large chromosomal regions, making these translocations impossible to analyse by standard PCR techniques. To experimentally prove that *MYC-IGH* spatial proximity favours generation of a translocation between the two loci, we created an experimental system for targeted generation of double strand breaks (DSBs) in the *MYC* and *IGH* loci: an RPMI8866-derived MYCIGHC9 cell line containing the *Cas9* gene and gRNAs targeting the *MYC* and *IGH* loci under the control of a Doxycycline (Dox)-inducible promoter (see Materials and Methods). In the presence of Dox, DSBs are specifically generated in the *MYC* and *IGH* loci. In some cells, erroneous repair of these DSBs by NHEJ generates the t(8;14) translocation. This translocation can then be detected and quantified by qPCR using a forward *MYC* primer and a reverse *IGH* primer, surrounding the chromosomal break(35) (Supplementary Fig. 5).

Cas9 expression started 3h after Dox treatment (Fig. 3a). Specific induction of DSBs was confirmed by colocalization between *MYC* and *IGH* loci and □H2AX foci (3D-FISH followed by □H2AX immunostaining). The damage in both loci peaked at 6h post-Dox treatment (Fig. 3b and c). We detected t(8;14) translocations by end-point PCR starting from 24h after Dox treatment (Fig. 3d). The more sensitive quantitative PCR was then applied to quantify the translocation rate. t(8;14) appeared already at 12h after Dox treatment ($0.8\pm0.24x10^{-3}$ cells), then the translocation rate increased at 24h ($7.2\pm0.54x10^{-3}$ cells; Fig. 3e) and peaked at 48h ($1.08\pm0.03x10^{-2}$ cells; Fig. 3e).

To get insight into the mechanism of the translocation generation in our system, we next used classical and alternative NHEJ (cNHEJ and aNHEJ, respectively) inhibitors. MYCIGHC9 cells treated with Dox were simultaneously incubated with either Mirin, an inhibitor of MRE11 (HR and NHEJ pathways) or NU7026 DNA-PK inhibitor (cNHEJ pathway) or L67 DNA ligase I and III inhibitor (aNHEJ pathway) and the t(8;14) translocation rate was measured by qPCR. Treatment with Mirin or L67 significantly decreased the t(8;14) translocation rate (fold change 0.60±0.02; $p<0.05$ for Mirin and 0.28±0.10; $p<0.01$ for L67; Fig. 3f) whereas treatment with NU7026 significantly increased the translocation frequency (fold change 3.68±0.13; $p<0.0001$; Fig. 3f). These results indicate that only inhibition of the aNHEJ pathway negatively impacts the t(8;14) translocation process and therefore suggests that, in our model, aNHEJ is a major pathway favouring the occurrence of translocations; this is consistent with previous results(36,37).

5. EBV reactivation-induced *MYC-IGH* spatial proximity increases the probability of t(8;14)

Using the MYCIGHC9 cell line, we next investigated whether an increased *MYC-IGH* proximity resulted in a higher t(8;14) translocation frequency. To this aim, MYCIGHC9 cells were first treated with either the recombinant Zebra protein or NaB for 48h to increase *MYC-IGH* proximity *via* EBV reactivation and then Cas9 and gRNAs expression was induced by addition of Dox. After additional 24 hours, cells were collected for t(8;14) quantification by qPCR (Fig. 4a). EBV reactivation with Zebra and NaB leads to the spatial proximity between the *MYC* and *IGH*, followed by a 2.07±0.28 and 3.72±0.56 fold increase in the translocation rate, respectively ($p<0.01$ and $p<0.001$; Fig. 4b). These data provide the first experimental

proof that gene proximity increases the probability of a chromosome translocation upon DSB induction.

6. Specific DNA damage within the *MYC* locus and MRE11 protein are involved in EBV-induced *MYC-IGH* spatial proximity

The increase in the colocalization rate between the *MYC* and *IGH* loci observed after EBV reactivation (Fig. 1b) could be a consequence of a displacement of one or both of these loci. Since DNA damage induction is one of the factors that can lead to loci movement within the nuclear space(20), we next analysed the proximity between the *IGH* and *MYC* loci in different conditions using several experimental systems.

We first used the MYCIGHC9 line to study *MYC* and *IGH* relative positioning following specific DSBs. We observed a significantly increased colocalization between these loci 48h after the DSB induction by Dox treatment (10.20%±1.67 in Dox treated cells vs 4.65%±0.34 in the control; $p<0.05$; OR 2.672 [1.063-7.052], $\chi^2=4.862$, p=0.0275; n≥120 cells, Fig. 4c). To test whether this *MYC-IGH* colocalization occurring after the introduction of DSBs within the *MYC* and *IGH* loci was specific, we analysed the *IGH* colocalization with another of its known translocation partners, *CCND1*(38) located on chromosome 11. Although a slight increase in the colocalization rate between the *CCND1* and *IGH* was observed 48h after Dox treatment of the MYCIGHC9 line, it was not statistically significant (9.23%±1.7 in Dox treated cells vs 6.54%±0.76 in the control; $p<0.05$; OR 1.319 [0.5525-3.082], $\chi^2=0.3739$, p=0.5409; n≥120 cells, Fig. 4d).

We next tested whether induction of a single DSB in either *MYC* or *IGH* locus would affect the proximity between the two genes by using the IGHC9 or MYCC9 cell lines where DSBs are induced only within the *IGH* or *MYC* loci, respectively. In Dox-treated IGHC9 cells we did not observe any increase in the *MYC-IGH* colocalization rate (3.86%±1.32 vs 4.28%±0.49 in the control; OR 1.129 [0.3778-3.330], $\chi^2=0.04843$, p=0.8258; n≥160 cells, Fig. 4e) whereas in MYCC9 cells, a significant increase in the *MYC-IGH* colocalization rate was detected (5.90%±0.11 vs 3.60%±0.06; $p<0.01$; OR 2.701 [1.161-6.514], $\chi^2=5.099$, p=0.0239; n≥85 cells Fig. 4f) suggesting that the DBS induction in the *MYC* locus triggers the colocalization.

In order to test whether DSB induction outside the target loci would affect the proximity between *MYC* and *IGH*, we have used the AMLETOC9 cell line with inducible expression of Cas9 and gRNA targeting the *ETO* and *AML* loci located on chromosomes 8 and 21, respectively. Induction of DSBs in these loci led to a slight decrease in the colocalization between the *MYC* and *IGH* loci (2.76%±0.92 in Dox treated cells vs 5.04%±0.39 in the control; OR 0.4449 [0.1229-1.661], $\chi^2=1.391$, p=0.2383; n≥100 cells, Fig. 4g).

Taken together, all these results suggest that in our experimental system, specific DNA damage within *MYC* locus, rather than within *IGH* locus is required for the *MYC-IGH* proximity to occur and as a consequence, it is quite likely that *MYC*, when damaged, moves toward the *IGH* locus.

Since the induction of EBV lytic cycle triggers DNA damage response in B cells (reviewed in (39)), and DNA damage within the *MYC* loci is an important factor for inducing *MYC-IGH* proximity, we next wanted to understand whether lytic cycle induction in RPMI8866 cells

caused DNA damage within the *MYC* locus. We induced EBV lytic cycle by treating cells with the recombinant Zebra protein and quantified the percentage of cells showing specific DNA damage within at least one *MYC* locus by measuring the colocalization between *MYC* loci and γH2AX foci using immuno-3D FISH. DNA damage within the *MYC* loci was also analysed in the M81 and rMSHJ cell lines that present spontaneous EBV reactivation. Both induced and spontaneous EBV reactivation were associated with an increased level of DNA damage within the *MYC* locus (27.48%±4.01 in Zebra-treated RPMI8866 cells; 23.99%±2.30 in M81 cells; 19.00%±1.37 in rMSHJ cells vs 9.41%±2.23 in RPMI8866 unstimulated cells; $p<0.01$; $p<0.001$; $p<0.01$ respectively; n≥380 cells Fig. 5a,5b). As simultaneous DNA damage in the *MYC* and *IGH* loci is required to generate the t(8;14) translocation, we also checked for the presence of DNA damage within the *IGH* locus in the same cells. After EBV reactivation, we observed a higher rate of DNA damage within the *IGH* locus as compared to the control RPMI8866 (data not shown). Simultaneous DNA damage within the *MYC* and *IGH* loci when they are located close to each other was also detected and even if this observation is not statistically significant, it illustrates the fact that DSBs can occur simultaneously within both loci when they are in close proximity. This may increase the risk of chromosomal translocations. Representative images of simultaneous DNA damage within the *MYC* and *IGH* loci following EBV reactivation are shown in Supplementary Fig. 6.

MRE11, one of the components of the DNA repair machinery, was shown to be involved in the movement of chromatin loci(26,40). We next explored a potential role of MRE11 in loci displacement in our model. First, we showed that EBV reactivation was accompanied by an increase in *MRE11* gene expression measured by qRT-PCR (fold change 1.68±0.11 in Zebra-treated RPMI8866 cells; 1.57±0.11 in M81 cells and 2.40±0.16 in rMSHJ cells vs unstimulated RPMI 8866 cells; $p<0.001$; $p<0.01$ and $p<0.0001$ respectively; Fig. 5c). We also observed that MRE11 inhibition by Mirin blocked the increase in *MYC-IGH* proximity induced by EBV reactivation (6.93%±1.08 in Zebra+Mirin treated cells vs 10.49%±1.16 in Zebra treated cells) (Fig. 5d). In contrast, inhibition of DNA-PK (involved in the cNHEJ) by NU7026, of Rad51 (involved in homologous recombination) by B02 or of Ligase III (involved in aNHEJ) by L67 did not affect the *MYC-IGH* colocalization (10.2%±2.6 in Zebra+NU7026 treated cells; 13.16%±1.79 in Zebra+B02-treated cells; 16.28%±2.16 in Zebra+L67-treated cells vs 10.49%±1.16 in Zebra-treated cells, n≥100 cells) (Fig. 5d). We also demonstrated that Mirin reduced the *MYC-IGH* colocalization rate in the MYCIGHC9 cells upon DNA damage induction in the *MYC* and *IGH* loci (5.42%±0,92 in Dox+Mirin treated cells vs 8.87%±0.89 in Dox treated cells, n≥90 cells) (Supplementary Fig. 7). Taken together, these data suggest that MRE11 could drive *MYC* displacement towards *IGH* following lytic cycle induction.

Discussion

The productive EBV lytic cycle increases the pool of infected B cells, but its intrinsic oncogenic effect is hardly conceivable due to the ensuing cell death(41); however an abortive (incomplete) lytic cycle which does not lead to the cell lysis(13,42–45) may be involved in EBV-associated cancers (reviewed in(10,45)). During latency, EBV latent proteins induce *MYC* expression through a reconfiguration of the DNA loop domains formed by *MYC* and its specific enhancers(46,47). Upon reactivation, the Zebra lytic protein blocks MYC expression(48) and the level of MYC protein controls the switch from latency to lytic cycle by negatively regulating *BZLF1*(49). Therefore, MYC downregulation required for lytic

cycle activation might involve suppression of the DNA loops between MYC locus and its enhancers and could explain the *MYC* locus movement suggested in our study. However, the reason why specific DNA damage within the *MYC* locus occurs during EBV reactivation remains an open question.

BL is one of the most common EBV-related diseases. Here we provide the first direct evidence that EBV lytic cycle predisposes to the appearance of the BL-specific t(8;14) chromosomal translocation. We found that both spontaneous and induced EBV reactivation led to a significant increase in the proportion of B cells showing the proximity between the *MYC* and *IGH* loci, otherwise located distantly in the nuclear space (Fig. 1b, Supplementary Fig. 1d, Fig. 1g). We also characterised here a rare case of primary EBV infection in an elderly patient caused by a kidney transplant from an EBV+ donor into the EBV- recipient (P1, Table 1). In this patient, B cells undergoing EBV lytic cycle had a prominent increase in *MYC-IGH* colocalization (Fig. 2). The development of BL is a possible scenario in post-transplant settings; these BLs have a high frequency of EBV positivity and a high mortality rate (50–53).

MYC and *IGH* spatial proximity and simultaneous DSBs on the two loci are prerequisites for t(8;14) generation; however it has never been experimentally shown that their proximity leads to translocation. We developed a cell line where simultaneous breaks within the *MYC* and the *IGH* loci can be induced, leading to t(8;14) detectable and measurable by qPCR. In this model, by inducing *MYC-IGH* proximity through EBV reactivation prior to DSBs, we were able to provide the first direct experimental proof that increased *MYC-IGH* proximity leads to an increased t(8;14) rate (Fig. 4).

We next demonstrated that specific DNA damage within the *MYC* locus could be a driving factor for the *MYC-IGH* proximity (Fig. 5). Consistently, we showed that EBV reactivation significantly increased the rate of DNA damage within the *MYC* locus. (Fig. 6a). Finally, our results point to a role for the DNA repair protein MRE11 in the *MYC* locus displacement. The *MRE11* gene is overexpressed upon EBV reactivation (Fig. 6c) and MRE11 inhibition after EBV reactivation or induced-DSB on *MYC* locus almost halved the *MYC-IGH* proximity (Fig. 6d and Supplementary Fig. 7). These results are in agreement with data from other studies implicating MRE11 in the relocation of damaged DNA loci(26,40,54,55).

We have previously demonstrated that HIV-1 transactivator protein Tat induced *MYC-IGH* proximity in primary B cells *in vitro* and *in vivo*(26). Unlike Zebra, the presence of Tat alone is able to promote *MYC-IGH* proximity; but despite this difference, the generation of DNA damage within the *MYC* locus and its MRE11-dependent relocalization in the nucleus are observed in both cases. Consistently, DNA DSBs have already been linked to chromatin movement(20,56,57), either for the search of a recombination partner(58,59) or to join the DNA repair centers(54,60). The increased chromatin movement following DSBs may lead to translocations(55).

In our system, DSBs were artificially generated by CRISPR/Cas9. In B cells, the main source of DSBs in the *MYC* and *IGH* loci is the activation-induced deaminase (AID)(61) involved in somatic hypermutation and class switch recombination(62,63). Although AID has a specific affinity for immunoglobulin genes, it is also able to target a large number of other genes (~25% of all expressed genes in B-cells)(64). AID was observed to associate with the *MYC* and *IGH* loci and to produce DSBs(65–67). Importantly, AID is localized in B cells in a discrete “recombination compartment” where it colocalizes with the *IGH* locus(68). Thus, colocalization of the *MYC* and *IGH* loci that we observed upon EBV reactivation might increase the probability of simultaneous AID-induced DSBs and thus t(8;14).

The important role played by EBV lytic cycle in BL development described in this work can be correlated with the fact that African children with an EBV-reactivated serological profile are more likely to develop endemic BL(69). Moreover, endemic EBV cofactors (*Plasmodium falciparum*, *Euphorbia tirucalli* and aflatoxin B1) induce EBV reactivation(70–72). Children living in EBV endemic areas and exposed to these cofactors, undergo repeated EBV reactivation with a subsequent increased *MYC-IGH* proximity in their B cells. The oncogenic t(8;14) could then occur upon simultaneous DNA damage, e.g. by AID(73–75).

Conclusions

In summary, we provide the first evidence that EBV reactivation triggered *MYC* and *IGH* spatial proximity *in vitro* and in patients; this proximity increased the t(8;14) rate after DSB induction in the *MYC* and *IGH* loci. Finally, we suggested a role for the MRE11 protein in the *MYC* locus displacement next to the *IGH* locus.

Methods

Cells

RPMI8866, PRIESS, M81 and rMSHJ human EBV-transformed lymphoblastoid cell lines (LCLs) were used in this study. M81 and rMSHJ are LCLs generated with recombinant M81 and MSHJ EBV strains respectively isolated from a Chinese Nasopharyngeal Carcinoma and a German Stem Cell Transplant recipient (32). We also created RPMI8866-derived cell lines that inducibly expressed CRISPR/Cas9 and guide RNAs (gRNAs), targeting both *MYC* and *IGH*; *MYC* only; *IGH* only or both *AML* and *ETO* loci. These RMPI8866-derived cell lines were named MYCIGHC9, MYCC9, IGHC9 and AMLETOC9, respectively. Cells were transfected and gRNAs efficiency was tested exploiting techniques and protocols developed in the laboratory (35,76). The sequences of gRNAs are listed in Supplementary table 1. Primary human B cells were isolated from blood of healthy donors by negative selection from total PBMCs. Cells were treated as described in Supplementary Table 2. See supplementary Materials and Methods for details.

Patients

Three patients were included in the study after obtaining an informed consent and a review by the local ethic committee (IMMUNOLYMPH protocol, CLEA-2020-113). All patients were diagnosed with HIV-negative EBV-related lymphoproliferative disorders. Detailed information on patients' history can be found in Table 1 and Supplementary Material and Methods Section.

Western blot

Cell pellets were resuspended in the NETN buffer and sonicated. Proteins (30 µg) were resolved on 4-12% SDS-PAGE gels, transferred onto a PVDF membrane and probed with the following primary antibodies: mouse anti-Cas9; mouse anti-Zebra; rabbit anti-□-tubulin and mouse anti-□-actin. Secondary HRP-conjugated antibodies were used to reveal bands. Western blot band intensity quantification was performed using the ImageJ software. The band intensity of a target protein was normalized to the band intensity of the indicated loading control protein.

Quantitative PCR and RT-PCR

Total DNA was extracted using Nucleospin® Tissue DNA purification kit (Macherey- Nagel) according to the manufacturer's protocol. Five hundred ng genomic DNA was amplified using primers specific for the t(8;14) translocation and control primers designed ~6.5 kbp downstream of the breakpoint sequence in the *MYC* gene locus. For RT-PCR, total RNA was extracted using Nucleospin® RNA II purification kit (Macherey- Nagel) according to the manufacturer's protocol. cDNA synthesis was performed as previously described(77). PCR amplification was performed using the PowerUp SYBR Green Master Mix (Thermo Scientific) following the manufacturer's protocol. The $2^{-\Delta\Delta Ct}$ method was used for quantification. Primer sequences are listed in Supplementary Table 3.

3D-FISH, Immuno-3D FISH, microscope image acquisition and analysis

Cells were processed for 3D-FISH or immuno-3D-FISH as previously described(26). Nuclei were counterstained with DAPI. Images were acquired using a multiphoton SP8 confocal microscope (Leica Microsystems, Berlin, Germany). Imaris software (Bitplane) was used to analyze gene localization. The LEICA Application Suite X (Leica Microsystems) software was used to evaluate the percentage of cells that have γH2AX foci colocalized with *MYC* and/or *IGH*. Mean BMRF1 nuclear intensity was analysed in ImageJ (see Supplementary methods).

Statistics

All statistical tests were performed using the Graphpad Prism 5 software (GraphPad software Inc., La Jolla, CA). One- way analysis of variance (ANOVA) test followed by Bonferroni's post-test or Student's t-test was used to compare averages between different groups. For binary comparisons of colocalization rate χ^2 test was also used, odds ratio (OR) [95% confidence interval], χ^2 value and p-value are provided. Two-way ANOVA followed by Bonferroni's post-test was used to compare averages for multiple-group comparisons with two factors (cell cycle and proliferation data). Data are presented as mean ± standard error of mean (SEM).

References

1. Brady G, MacArthur GJ, Farrell PJ. Epstein-Barr virus and Burkitt lymphoma. J Clin Pathol. 2007;60:1397–402.
2. Bornkamm GW. Epstein-Barr virus and the pathogenesis of Burkitt's lymphoma: more questions than answers. Int J Cancer. 2009;124:1745–55.
3. Moormann AM, Bailey JA. Malaria - how this parasitic infection aids and abets EBV-associated Burkitt lymphomagenesis. Curr Opin Virol. 2016;20:78–84.
4. Mawson AR, Majumdar S. Malaria, Epstein-Barr virus infection and the pathogenesis of Burkitt's lymphoma. Int J Cancer. 2017;141:1849–55.
5. Amon W, Farrell PJ. Reactivation of Epstein-Barr virus from latency. Rev Med Virol. 2005;15:149–56.
6. Cohen JI. Epstein-Barr virus infection. N Engl J Med. 2000;343:481–92.
7. Epstein MA, Henle G, Achong BG, Barr YM. MORPHOLOGICAL AND BIOLOGICAL STUDIES ON A VIRUS IN CULTURED LYMPHOBLASTS FROM BURKITT'S LYMPHOMA. J Exp Med. 1965;121:761–70.
8. Tsurumi T, Fujita M, Kudoh A. Latent and lytic Epstein-Barr virus replication strategies.

Rev Med Virol. 2005;15:3–15.
9. Countryman J, Miller G. Activation of expression of latent Epstein-Barr herpesvirus after gene transfer with a small cloned subfragment of heterogeneous viral DNA. Proc Natl Acad Sci U S A. 1985;82:4085–9.
10. Germini D, Sall FB, Shmakova A, Wiels J, Dokudovskaya S, Drouet E, et al. Oncogenic Properties of the EBV ZEBRA Protein. Cancers (Basel). 2020;12.
11. Grogan E, Jenson H, Countryman J, Heston L, Gradoville L, Miller G. Transfection of a rearranged viral DNA fragment, WZhet, stably converts latent Epstein-Barr viral infection to productive infection in lymphoid cells. Proc Natl Acad Sci U S A. 1987;84:1332–6.
12. Murata T, Tsurumi T. Switching of EBV cycles between latent and lytic states. Rev Med Virol. 2014;24:142–53.
13. Al Tabaa Y, Tuaillon E, Bollore K, Foulongne V, Petitjean G, Seigneurin J-M, et al. Functional Epstein-Barr virus reservoir in plasma cells derived from infected peripheral blood memory B cells. Blood. 2009;113:604–11.
14. Robinson M, Schor S, Barouch-Bentov R, Einav S. Viral journeys on the intracellular highways. Cell Mol Life Sci. 2018;75:3693–714.
15. Rosemarie Q, Sugden B. Epstein-Barr Virus: How Its Lytic Phase Contributes to Oncogenesis. Microorganisms. 2020;8.
16. Allday MJ. How does Epstein-Barr virus (EBV) complement the activation of Myc in the pathogenesis of Burkitt's lymphoma? Semin Cancer Biol. 2009;19:366–76.
17. Molyneux EM, Rochford R, Griffin B, Newton R, Jackson G, Menon G, et al. Burkitt's lymphoma. Lancet. 2012;379:1234–44.
18. Saleh K, Michot J-M, Camara-Clayette V, Vassetsky Y, Ribrag V. Burkitt and Burkitt-Like Lymphomas: a Systematic Review. Curr Oncol Rep. 2020;22:33.
19. Torgbor C, Awuah P, Deitsch K, Kalantari P, Duca KA, Thorley-Lawson DA. A multifactorial role for P. falciparum malaria in endemic Burkitt's lymphoma pathogenesis. PLoS Pathog. 2014;10:e1004170.
20. Iarovaia OV, Rubtsov M, Ioudinkova E, Tsfasman T, Razin SV, Vassetzky YS. Dynamics of double strand breaks and chromosomal translocations. Mol Cancer. 2014;13:249.
21. Roix JJ, McQueen PG, Munson PJ, Parada LA, Misteli T. Spatial proximity of translocation-prone gene loci in human lymphomas. Nat Genet. 2003;34:287–91.
22. Roukos V, Burman B, Misteli T. The cellular etiology of chromosome translocations. Curr Opin Cell Biol. 2013;25:357–64.
23. Sall FB, Germini D, Kovina AP, Ribrag V, Wiels J, Toure AO, et al. Effect of Environmental Factors on Nuclear Organization and Transformation of Human B Lymphocytes. Biochemistry (Mosc). 2018;83:402–10.
24. Nijland M, Kersten MJ, Pals S, Bemelman F, ten Berge I. Epstein-Barr Virus–Positive Posttransplant Lymphoproliferative Disease After Solid Organ Transplantation: Pathogenesis, Clinical Manifestations, Diagnosis, and Management. Transplantation Direct. 2016;2:e48.
25. Pannunzio NR, Watanabe G, Lieber MR. Nonhomologous DNA end-joining for repair of DNA double-strand breaks. J Biol Chem. 2018;293:10512–23.
26. Germini D, Tsfasman T, Klibi M, El-Amine R, Pichugin A, Iarovaia OV, et al. HIV Tat induces a prolonged MYC relocalization next to IGH in circulating B-cells. Leukemia. 2017;31:2515–22.
27. Sklyar I, Iarovaia OV, Gavrilov AA, Pichugin A, Germini D, Tsfasman T, et al. Distinct Patterns of Colocalization of the CCND1 and CMYC Genes With Their Potential Translocation Partner IGH at Successive Stages of B-Cell Differentiation. Journal of Cellular Biochemistry. 2016;117:1506–10.
28. Kim K-D, Tanizawa H, De Leo A, Vladimirova O, Kossenkov A, Lu F, et al. Epigenetic specifications of host chromosome docking sites for latent Epstein-Barr virus. Nature Communications. Nature Publishing Group; 2020;11:877.
29. Li C, Shi Z, Zhang L, Huang Y, Liu A, Jin Y, et al. Dynamic changes of territories 17

and 18 during EBV-infection of human lymphocytes. Mol Biol Rep. 2009/08/18 ed. 2010;37:2347–54.
30. Moquin SA, Thomas S, Whalen S, Warburton A, Fernandez SG, McBride AA, et al. The Epstein-Barr Virus Episome Maneuvers between Nuclear Chromatin Compartments during Reactivation. J Virol [Internet]. 2018 [cited 2021 Jan 26];92. Available from: https://www.ncbi.nlm.nih.gov/pmc/articles/PMC5774889/
31. Osborne CS, Chakalova L, Mitchell JA, Horton A, Wood AL, Bolland DJ, et al. Myc Dynamically and Preferentially Relocates to a Transcription Factory Occupied by Igh. Susan M Gasser, editor. PLoS Biol. 2007;5:e192.
32. Delecluse S, Poirey R, Zeier M, Schnitzler P, Behrends U, Tsai M-H, et al. Identification and Cloning of a New Western Epstein-Barr Virus Strain That Efficiently Replicates in Primary B Cells. J Virol. 2020;94.
33. Tsai M-H, Raykova A, Klinke O, Bernhardt K, Gärtner K, Leung CS, et al. Spontaneous lytic replication and epitheliotropism define an Epstein-Barr virus strain found in carcinomas. Cell Rep. 2013;5:458–70.
34. Küppers R, Dalla-Favera R. Mechanisms of chromosomal translocations in B cell lymphomas. Oncogene. 2001;20:5580–94.
35. Germini D, Bou Saada Y, Tsfasman T, Osina K, Robin C, Lomov N, et al. A One-Step PCR-Based Assay to Evaluate the Efficiency and Precision of Genomic DNA-Editing Tools. Mol Ther Methods Clin Dev. 2017;5:43–50.
36. Simsek D, Jasin M. Alternative end-joining is suppressed by the canonical NHEJ component Xrcc4-ligase IV during chromosomal translocation formation. Nat Struct Mol Biol. 2010;17:410–6.
37. Soni A, Siemann M, Pantelias GE, Iliakis G. Marked contribution of alternative end-joining to chromosome-translocation-formation by stochastically induced DNA double-strand-breaks in G2-phase human cells. Mutat Res Genet Toxicol Environ Mutagen. 2015;793:2–8.
38. Vogt N, Dai B, Erdmann T, Berdel WE, Lenz G. The molecular pathogenesis of mantle cell lymphoma. Leuk Lymphoma. 2017;58:1530–7.
39. Hau PM, Tsao SW. Epstein–Barr Virus Hijacks DNA Damage Response Transducers to Orchestrate Its Life Cycle. Viruses [Internet]. 2017 [cited 2021 Jan 9];9. Available from: https://www.ncbi.nlm.nih.gov/pmc/articles/PMC5707548/
40. Caridi CP, D'Agostino C, Ryu T, Zapotoczny G, Delabaere L, Li X, et al. Nuclear F-actin and myosins drive relocalization of heterochromatic breaks. Nature. 2018;559:54–60.
41. Münz C. Latency and lytic replication in Epstein–Barr virus-associated oncogenesis. Nature Reviews Microbiology. 2019;17:691–700.
42. Arvey A, Tempera I, Tsai K, Chen H-S, Tikhmyanova N, Klichinsky M, et al. An Atlas of the Epstein-Barr Virus Transcriptome and Epigenome Reveals Host-Virus Regulatory Interactions. Cell Host & Microbe. 2012;12:233–45.
43. Chiu Y-F, Sugden B. Epstein-Barr Virus: The Path from Latent to Productive Infection. Annu Rev Virol. 2016;3:359–72.
44. Ersing I, Nobre L, Wang LW, Soday L, Ma Y, Paulo JA, et al. A Temporal Proteomic Map of Epstein-Barr Virus Lytic Replication in B Cells. Cell Reports. 2017;19:1479–93.
45. Morales-Sánchez A, Fuentes-Panana E. The Immunomodulatory Capacity of an Epstein-Barr Virus Abortive Lytic Cycle: Potential Contribution to Viral Tumorigenesis. Cancers. 2018;10:98.
46. Wood CD, Veenstra H, Khasnis S, Gunnell A, Webb HM, Shannon-Lowe C, et al. MYC activation and BCL2L11 silencing by a tumour virus through the large-scale reconfiguration of enhancer-promoter hubs. Elife. 2016;5:e18270.
47. Jiang S, Zhou H, Liang J, Gerdt C, Wang C, Ke L, et al. The Epstein-Barr Virus Regulome in Lymphoblastoid Cells. Cell Host Microbe. 2017;22:561-573.e4.
48. Rodriguez A, Jung EJ, Yin Q, Cayrol C, Flemington EK. Role of c-myc regulation in Zta-mediated induction of the cyclin-dependent kinase inhibitors p21 and p27 and cell growth arrest. Virology. 2001;284:159–69.
49. Guo R, Jiang C, Zhang Y, Govande A, Trudeau SJ, Chen F, et al. MYC Controls the

Epstein-Barr Virus Lytic Switch. Mol Cell. 2020;78:653-669.e8.
50. Ferreiro JF, Morscio J, Dierickx D, Marcelis L, Verhoef G, Vandenberghe P, et al. Post-transplant molecularly defined Burkitt lymphomas are frequently MYC-negative and characterized by the 11q-gain/loss pattern. Haematologica. 2015;100:e275–9.
51. Djokic M, Le Beau MM, Swinnen LJ, Smith SM, Rubin CM, Anastasi J, et al. Post-transplant lymphoproliferative disorder subtypes correlate with different recurring chromosomal abnormalities. Genes, Chromosomes and Cancer. 2006;45:313–8.
52. Picarsic J, Jaffe R, Mazariegos G, Webber SA, Ellis D, Green MD, et al. Post-transplant Burkitt lymphoma is a more aggressive and distinct form of post-transplant lymphoproliferative disorder. Cancer. 2011;117:4540–50.
53. Akar Özkan E, Özdemir BH, Akdur A, Deniz EE, Haberal M. Burkitt lymphoma after transplant: an aggressive lymphoproliferative disease. Exp Clin Transplant. 2014;12 Suppl 1:136–8.
54. Aten JA, Stap J, Krawczyk PM, van Oven CH, Hoebe RA, Essers J, et al. Dynamics of DNA double-strand breaks revealed by clustering of damaged chromosome domains. Science. 2004;303:92–5.
55. Roukos V, Voss TC, Schmidt CK, Lee S, Wangsa D, Misteli T. Spatial dynamics of chromosome translocations in living cells. Science. 2013;341:660–4.
56. Krawczyk PM, Borovski T, Stap J, Cijsouw T, ten Cate R, Medema JP, et al. Chromatin mobility is increased at sites of DNA double-strand breaks. J Cell Sci. 2012;125:2127–33.
57. Kruhlak MJ, Celeste A, Dellaire G, Fernandez-Capetillo O, Müller WG, McNally JG, et al. Changes in chromatin structure and mobility in living cells at sites of DNA double-strand breaks. J Cell Biol. 2006;172:823–34.
58. Miné-Hattab J, Chiolo I. Complex Chromatin Motions for DNA Repair. Front Genet. 2020;11:800.
59. Miné-Hattab J, Rothstein R. Increased chromosome mobility facilitates homology search during recombination. Nat Cell Biol. 2012;14:510–7.
60. Neumaier T, Swenson J, Pham C, Polyzos A, Lo AT, Yang P, et al. Evidence for formation of DNA repair centers and dose-response nonlinearity in human cells. Proc Natl Acad Sci U S A. 2012;109:443–8.
61. Honjo T, Kinoshita K, Muramatsu M. Molecular mechanism of class switch recombination: linkage with somatic hypermutation. Annu Rev Immunol. 2002;20:165–96.
62. Chaudhuri J, Basu U, Zarrin A, Yan C, Franco S, Perlot T, et al. Evolution of the immunoglobulin heavy chain class switch recombination mechanism. Adv Immunol. 2007;94:157–214.
63. Di Noia JM, Neuberger MS. Molecular mechanisms of antibody somatic hypermutation. Annu Rev Biochem. 2007;76:1–22.
64. Liu M, Duke JL, Richter DJ, Vinuesa CG, Goodnow CC, Kleinstein SH, et al. Two levels of protection for the B cell genome during somatic hypermutation. Nature. 2008;451:841–5.
65. Boerma EG, Siebert R, Kluin PM, Baudis M. Translocations involving 8q24 in Burkitt lymphoma and other malignant lymphomas: a historical review of cytogenetics in the light of todays knowledge. Leukemia. 2009;23:225–34.
66. Duquette ML, Pham P, Goodman MF, Maizels N. AID binds to transcription-induced structures in c-MYC that map to regions associated with translocation and hypermutation. Oncogene. 2005;24:5791–8.
67. Yu K, Chedin F, Hsieh C-L, Wilson TE, Lieber MR. R-loops at immunoglobulin class switch regions in the chromosomes of stimulated B cells. Nat Immunol. 2003;4:442–51.
68. Pichugin A, Iarovaia OV, Gavrilov A, Sklyar I, Barinova N, Barinov A, et al. The IGH locus relocalizes to a “recombination compartment” in the perinucleolar region of differentiating B-lymphocytes. Oncotarget. 2017;8:40079–89.
69. Coghill AE, Proietti C, Liu Z, Krause L, Bethony J, Prokunina-Olsson L, et al. The Association between the Comprehensive Epstein-Barr Virus Serologic Profile and

Endemic Burkitt Lymphoma. Cancer Epidemiol Biomarkers Prev. 2020;29:57–62.
70. Accardi R, Gruffat H, Sirand C, Fusil F, Gheit T, Hernandez-Vargas H, et al. The mycotoxin aflatoxin B1 stimulates Epstein-Barr virus-induced B-cell transformation in in vitro and in vivo experimental models. Carcinogenesis. 2015;36:1440–51.
71. Chêne A, Donati D, Guerreiro-Cacais AO, Levitsky V, Chen Q, Falk KI, et al. A molecular link between malaria and Epstein-Barr virus reactivation. PLoS Pathogens. 2007;3:0826–34.
72. MacNeil A, Sumba OP, Lutzke ML, Moormann A, Rochford R. Activation of the Epstein-Barr virus lytic cycle by the latex of the plant Euphorbia tirucalli. Br J Cancer. 2003;88:1566–9.
73. Robbiani DF, Bothmer A, Callen E, Reina-San-Martin B, Dorsett Y, Difilippantonio S, et al. AID is required for the chromosomal breaks in c-myc that lead to c-myc/IgH translocations. Cell. 2008;135:1028–38.
74. Ramiro AR, Jankovic M, Eisenreich T, Difilippantonio S, Chen-Kiang S, Muramatsu M, et al. AID is required for c-myc/IgH chromosome translocations in vivo. Cell. 2004;118:431–8.
75. Dorsett Y, Robbiani DF, Jankovic M, Reina-San-Martin B, Eisenreich TR, Nussenzweig MC. A role for AID in chromosome translocations between c-myc and the IgH variable region. The Journal of Experimental Medicine. 2007;204:2225–32.
76. Canoy RJ, André F, Shmakova A, Wiels J, Lipinski M, Vassetzky Y, et al. Easy and robust electrotransfection protocol for efficient ectopic gene expression and genome editing in human B cells. Gene Ther. 2020;
77. Sall FB, El Amine R, Markozashvili D, Tsfasman T, Oksenhendler E, Lipinski M, et al. HIV- 1 Tat protein induces aberrant activation of *AICDA* in human B- lymphocytes from peripheral blood. J Cell Physiol. 2019;234:15678–85.

Abbreviations

AMLETOC9: RPMI8866-derived cell line that inducibly express CRISPR/Cas9 and gRNAs, targeting both *AML* and *ETO* loci
aNHEJ: alternative NHEJ
ANOVA: analysis of variance
BL: Burkitt's lymphoma
BLLF BamHI- L fragment leftward open reading frame
BMRF: BamHI- M fragment rightward open reading frame
BRLF: BamHI- R fragment leftward open reading frame
BZLF: BamH1- Z fragment leftward open reading frame
Cas9: CRISPR associated protein 9
cNHEJ: classical NHEJ
CRISPR: clustered regularly interspaced short palindromic repeats
Dox: doxycycline
DSB: Double strand break
EBV: Epstein- Barr Virus
FISH: fluorescence in situ hybridization
gRNA: guide RNA
HIV: human immunodeficiency virus
HR: homologous recombination
IGH: immunoglobulin heavy chain
IGHC9: RPMI8866-derived cell line that inducibly express CRISPR/Cas9 and gRNA, targeting both *IGH* locus

LCL: lymphoblastoid cell line
MYCIGHC9: RPMI8866-derived cell line that inducibly express CRISPR/Cas9 and gRNAs, targeting both *MYC* and *IGH* loci
MYCC9: RPMI8866-derived cell line that inducibly express CRISPR/Cas9 and gRNA, targeting both *MYC* locus
NaB: sodium butyrate
NHEJ: non-homologous end-joining

Acknowledgements

M81 and rMSHJ are a kind gift from Henri-Jacques Delecluse (DKFZ, Heidelberg, Germany)). The authors thank Tudor Manoliu, Gustave Roussy Cancer Campus, Plateforme Imagerie et Cytométrie - UMS 23/3655 - Université Paris Saclay, Villejuif, France for technical help.

Funding

This study was supported by grants from the INSERM (ENVIBURKITT), La Ligue Contre le Cancer (M27231) and the IDB RAS government basic research program 0088-2021-0007. FBS was a recipient of the grants from the Institut Servier and Service de coopération et d'action culturelle de l'Ambassade de France au Sénégal. AK is a recipient of the Eiffel Fellowship from Campus France. This study was supported by a grant from TA2019 and TA2021, Univ. Paris Sud, université Paris Saclay, France.

Author information

Affiliations

UMR9018, Université Paris-Saclay, CNRS, Gustave Roussy, Villejuif, France
Fatimata Bintou Sall, Anna Shmakova, Tatyana Tsfasman, Nikolai Lomov, Anna Karpukhina, Reynand Canoy, Marc Lipinski, Joëlle Wiels, Diego Germini, Yegor Vassetzky

Faculty of Medicine, Pharmacy and Odontology, Cheikh Anta Diop University of Dakar, Senegal
Fatimata Bintou Sall, Awa Oumar Toure

Laboratory of Molecular Endocrinology, Institute of Experimental Cardiology, Federal State Budgetary Organization National Cardiology Research Center Ministry of Health of the Russian Federation, Moscow, Russia
Anna Shmakova

Koltzov Institute of Developmental Biology, Russian Academy of Sciences, Moscow, Russia
Anna Shmakova, Anna Karpukhina, Yegor Vassetzky

Faculty of Biology, State University of Moscow, Russia
Nikolai Lomov

Service d'Immunopathologie Clinique, Hôpital St Louis, APHP, 75012 Paris, France
David Boutboul, Eric Oksenhendler

Contributions

F.B.S., A.S., D.G. performed research, analyzed data and wrote the paper; T.T. and N.L. performed research and contributed new reagents; A.K. and R.J.C. performed research; A.O.T. and M.L. analyzed data; J.W. analyzed data, and wrote the paper; D.B. and E.O. provided samples from patients and clinical data; Y.V. designed research, analyzed data and wrote the paper.

Corresponding authors

Correspondence to Yegor Vassetzky or Diego Germini

Ethics declarations

Three patients were included in the study after obtaining an informed consent and a review by the local ethic committee (IMMUNOLYMPH protocol, CLEA-2020-113).

Consent for publication

Consent for publication has been obtained from the patients.

Tables

Table 1. Patients' characteristics. All patients were diagnosed with HIV-negative EBV-related lymphoproliferative disorders.

Patient	Diagnosis	Treatment	Age	Gender	Log PCR EBV in whole blood	% of B cells with *MYC-IGH* loci colocalization (n of cells analyzed)	*P* value compared to healthy donor B cells
P1	Severe post-transplant primary EBV infection	Steroids, rituximab, etoposide	74	M	6	21.46 (n=460)	<0.0001 ****
P2	Cerebral EBV+ polymorphic lymphoproliferative disorder related to prolonged iatrogenic immunosuppression (systemic lupus erythematosus)	Rituximab, cytarabine	43	F	3	16.67 (n=132)	0.0012 **
P3	Severe infectious mononucleosis with hemophagocytic lympho-histiocytosis	Steroids, etoposide, cyclosporin	23	F	8	11.63 (n=86)	ns

Table legends

Table 1. Patients' characteristics. All patients were diagnosed with HIV-negative EBV-related lymphoproliferative disorders.

Figure legends

Fig. 1. EBV reactivation in RPMI8866 induces *MYC-IGH* colocalization.

(a) The percentage of cells with colocalized *MYC-IGH* signals (i.e. cells where the distance between the centers of corresponding 3D-FISH signals was equal or less than 1 µm) in B cells purified from healthy donors (B cells), latent EBV-positive RPMI8866 untreated or treated with sodium butyrate (NaB) or Zebra recombinant protein to induce lytic cycle. 3D-FISH was performed 48h after treatment. A minimum of 100 cells from at least two different experiments and two technical replicates were analysed. (b) Representative optic section of a 3D-FISH image of RPMI8866 cells treated with the EBV lytic cycle inducer Zebra for 48h. Nuclei stained with DAPI are represented in blue, *MYC* and *IGH* gene loci stained with specific fluorescent probes are represented in red and green, respectively. Colocalization between the *MYC* and *IGH* loci is highlighted by the yellow arrow. Scale bar = 5 µm. The right panel shows *MYC* (red curve) and *IGH* (green curve) signal intensities along the white bar drawn in the MERGE picture. (c) Western blot analysis of Zebra protein cell entry into primary B cells purified from healthy donors and treated with 1 µg/ml recombinant Zebra for the indicated time. Control, untreated B cells. (d) *MYC-IGH* colocalization rate in B cells purified from healthy donors and treated with the recombinant Zebra protein for the indicated times. 3D-FISH was performed 24h and 48h after treatment. A minimum of 180 cells from at least two different experiments and two technical replicates were analysed. (e) *MYC-IGH* colocalization in primary B cells purified from healthy donors, activated with a cocktail of reagents (recombinant human IL4+ human CD40 monoclonal antibody+ anti-human IgM monoclonal antibody) and treated or not with the recombinant Zebra protein for 48h. A minimum of 60 cells were analysed. (f,g) Analysis of the expression of *BZLF1* (f) and *BRLF1* (g) by qRT-PCR in M81 and rMSHJ cell lines with spontaneous EBV lytic activity. Expression is presented, after normalization with *GAPDH* expression, as fold change in comparison to the unstimulated RPMI8866, set as 1. Data are from three experiments and two technical replicates. (h) *MYC-IGH* colocalization rate in M81 and rMSHJ cells with spontaneous lytic activity, in comparison to RPMI8866. A minimum of 200 cells from at least two different experiments and two technical replicates were analysed. (i) *MYC-IGH* colocalization in BMRF1 positive and BMRF1 negative M81 cells. M81 cells were processed for 3D-FISH targeting *MYC* and *IGH* loci and cells undergoing lytic cycle were identified by immunofluorescence staining of the EBV early lytic protein BMRF1. n>70 cells analysed per condition. (j) A representative immuno-3DFISH image of *MYC-IGH* colocalization occuring in a BMRF1 positive M81 cell. All data are plotted as mean±SEM. **p*<0.05; ** *p*<0.01; ****p*<0.001 as compared by ANOVA, Bonferroni's post-test for more than two groups or t-test for two groups.

Fig. 2. EBV reactivation in a patient with severe post-transplant primary EBV infection is associated with *MYC-IGH* colocalization.

(a) Representative image of immunofluorescent staining of the EBV early lytic protein BMRF1 in patient #1 B cells (P1). Nuclei stained with DAPI are represented in grey, BMRF1

in blue. Scale bar = 30 µm. (b) The percentage of cells with colocalized *MYC-IGH* signals (i.e. cells where the distance between the centres of corresponding 3D-FISH signals was equal or less than 1 µm) in B cells purified from healthy donors, in B cells purified from patient #1 with severe post-transplant primary EBV infection (P1) and in among BMRF1 positive (BMRF1+) B cells from patient #1. n>50 cells analysed per condition. Data are plotted as mean±SEM. ** $p<0.01$; **** $p<0.0001$ as compared by ANOVA, Bonferroni's post-test. (c) A representative immuno-3DFISH image of *MYC-IGH* colocalization occuring in a BMRF1 positive B cell.

Fig. 3. Induction of the t(8;14) in the MYCIGHC9 cell line.

(a) Representative image of western blot kinetic analysis of Dox-induced Cas9 expression. Alpha-tubulin was used as a protein loading control. (b, c) Induction of DNA damage within the *MYC* and *IGH* loci after Cas9 and gRNAs expression. Cells were treated with Dox for the indicated times and 3D-FISH was performed with *MYC* and *IGH* probes followed by γH2AX immunofluorescence staining. Percentage of cells with γH2AX foci colocalized with the *MYC* (b) or *IGH* loci (c) were obtained from at least two independent experiments where at least 150 cells were examined for each condition. (d, e) Kinetics of *MYC-IGH* translocation formation after Dox treatment. Cells were treated with Dox for the indicated times and collected for DNA extraction. End-point PCR followed by electrophoresis on agarose gel (d) or quantitative PCR (e) were performed. t(8;14) rates in (e) are calculated according to the following formula: translocation rate=$2x2^{-\Delta Ct\ of\ MYC\text{-}IGH\ and\ MYC\ amplicon}$ translocations per cell. The data represent results from three independent experiments and two technical replicates for each. (f) Effect of DNA repair inhibitors on the *MYC-IGH* translocation rate. Cells were simultaneously treated with Dox and the indicated inhibitor or left untreated for 24h and translocations were detected by qPCR. t(8;14) rate fold changes are calculated after normalization to the *MYC* gene in comparison to t(8;14) level in Dox-treated cells, set as 1. The data represent results from three independent experiments with two technical replicates for each. All data are plotted as mean±SEM. ns, non-significant; * $p<0.05$; ** $p<0.01$; *** $p<0.001$; **** $p<0.0001$ as compared by ANOVA, Bonferroni's post-test.

Fig. 4. EBV reactivation-induced *MYC-IGH* spatial proximity is favored by specific DNA damage in the *MYC* locus and increases the t(8;14) rate upon DSB induction within the *MYC* and *IGH* loci

(a) Experimental design. MYCIGHC9 line cells were treated or not with recombinant Zebra protein or sodium butyrate (NaB) for 48h to induce EBV reactivation and the consequent *MYC-IGH* proximity followed by Dox treatment for 24h and qPCR for *MYC-IGH* translocation detection. (b) qPCR for *MYC-IGH* translocation in Dox-treated cells after Zebra or NaB treatment. Fold changes in t(8;14) levels are calculated after normalization to the *MYC* gene in comparison to translocation rate in cells treated only with Dox, set as 1. The data represent results from three independent experiments with two technical replicates for each. (c) *MYC-IGH* colocalization rate in the MYCIGHC9 cell line. Cells were treated by Dox for 48h to induce the expression of Cas9 and gRNA targeting *MYC* and *IGH*. 3D-FISH was performed to evaluate the *MYC-IGH* spatial proximity. (d) *CCND1-IGH* colocalization rate in the MYCIGHC9 line after Cas9-induced DSBs in the *MYC* and *IGH* loci. The same cells as in (c) were used to evaluate the *IGH* proximity with the *CCND1* locus by 3D-FISH. (e) *MYC-IGH* colocalization rate in IGHC9 line after Cas9 induced DSB on *IGH* locus. (f) *MYC-IGH* colocalization rate in the *MYCC9* line after Cas9 induced DSB on *MYC* locus. (g) *MYC-IGH* colocalization in the AMLETOC9 line after simultaneous Cas9 induced DSB within the *AML* and *ETO* loci. A minimum of 85 cells from at least one experiment and at least three technical replicates were analysed for each 3D FISH experiment. All data are plotted as

mean ± SEM. ns, non-significant; *p<0.05; **p<0.01 as compared by ANOVA, Bonferroni's post-test (b) or by t-test (c-g).

Fig. 5. EBV reactivation induces DNA damage within the *MYC* locus and MRE11 is involved in *MYC* relocalization next to *IGH*.

(a) Representative slice-section of an immuno-3D-FISH image with colocalized γH2AX foci (represented in blue) and the *MYC* locus (in red). Scale bar = 5µm. The right panel illustrates *MYC* (red curve) and γH2AX (blue curve) colocalization (x-axis) along the white bar drawn in the MERGE picture, with the respective peak intensities (y-axis), Scale bar = 5µm. (b) DNA damage within the *MYC* locus in LCLs with the induced (RPMI8866+Zebra) or spontaneous (M81 and rMSHJ) lytic activity. Cells were processed for 3D-FISH followed by immunostaining for γH2AX. Y axis, percentage of cells with γH2AX foci colocalized with the *MYC* locus. A minimum of 380 cells from two experiments and at least three technical replicates were analysed. (c) *MRE11* expression analysed by qRT-PCR in LCLs with induced (RPMI8866+Zebra) or spontaneous (M81 and rMSHJ) lytic activity. *MRE11* expression fold changes upon EBV reactivation are calculated after normalization with *GAPDH* expression in comparison with *MRE11* expression in RPMI8866, set as 1. (d) *MYC-IGH* colocalization in RPMI8866 treated or not with recombinant Zebra protein for 48h, in association or not with the MRE11 inhibitor Mirin or the DNA-PK inhibitor NU7026 or the Rad51 inhibitor B02 or the DNA LigaseIII inhibitor L67. A minimum of 100 cells from two experiments and at least three technical replicates were analysed. All data are plotted as mean ± SEM. ns, non-significant; *p<0.05; **p<0.01; ***p<0.001; as compared by ANOVA, Bonferroni's post-test.

Figures

Fig. 1.

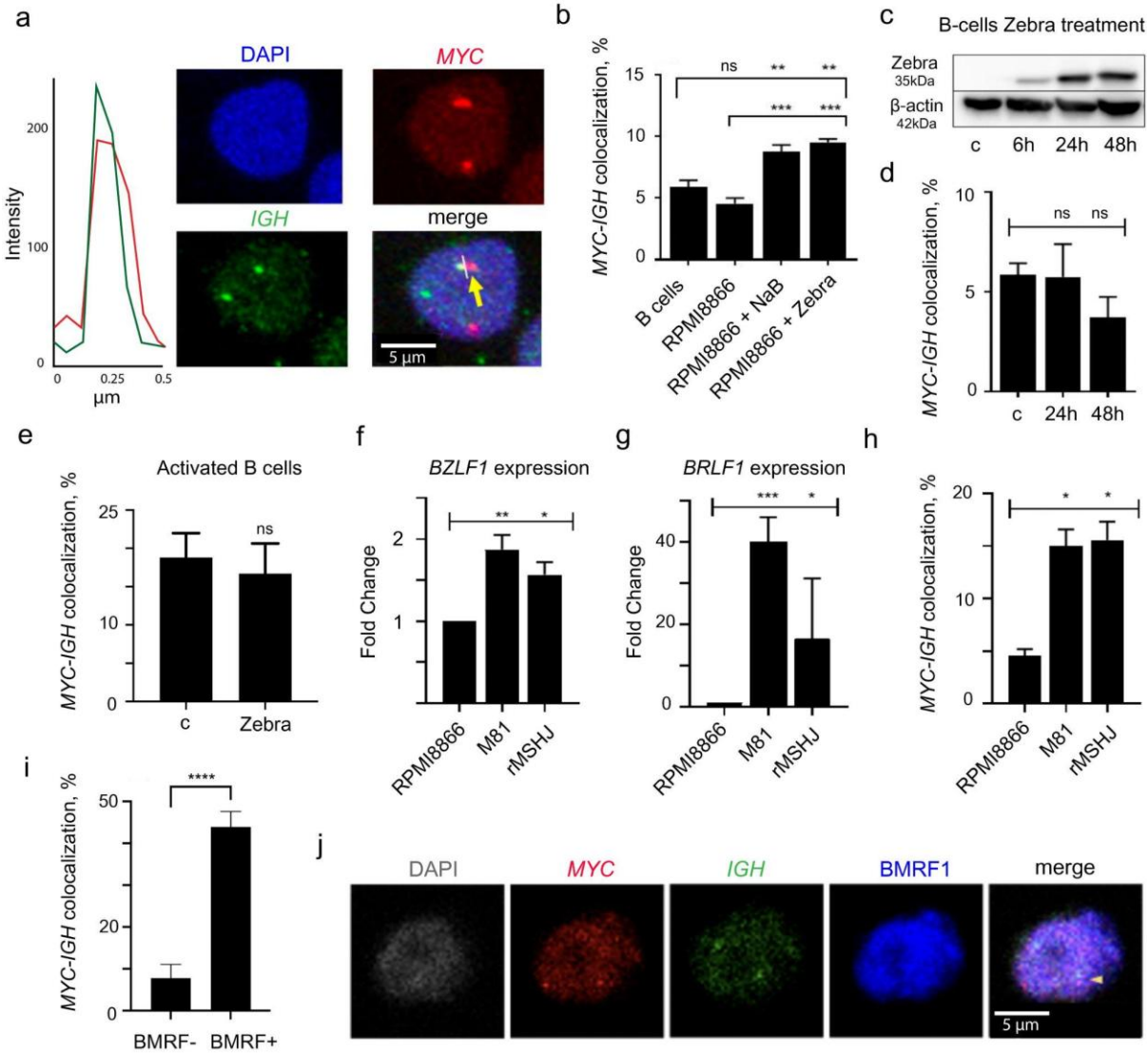

Fig. 2

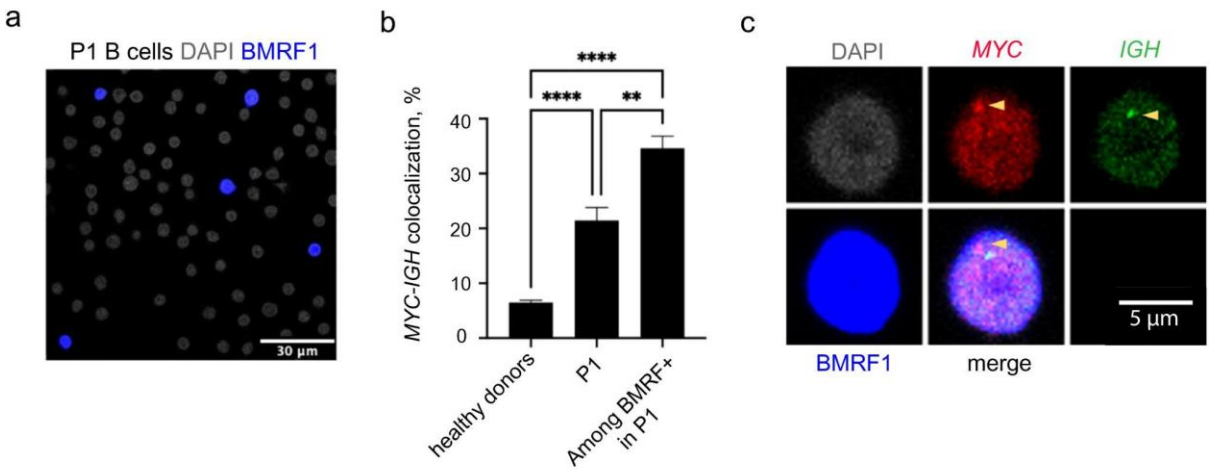
a
P1 B cells DAPI BMRF1
30 µm
b
MYC-IGH colocalization, %
****
****
**
healthy donors
P1
Among BMRF+ in P1
c
DAPI
MYC
IGH
5 µm
BMRF1
merge

Fig. 3

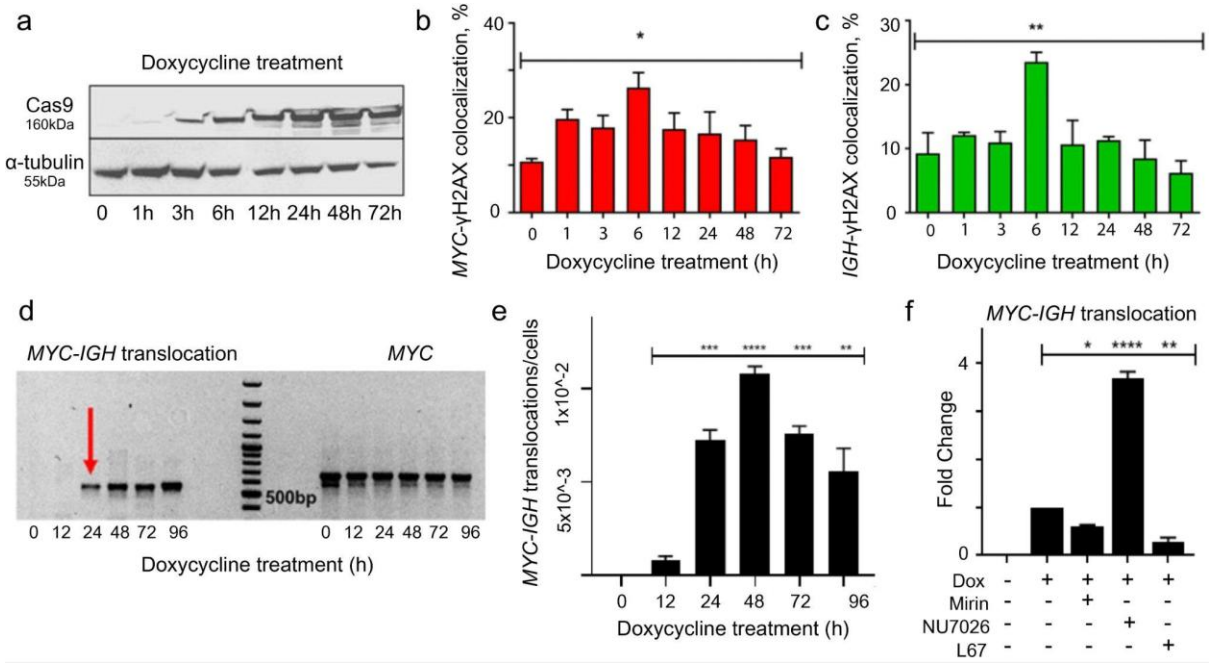
a
Doxycycline treatment
Cas9
160kDa
α-tubulin
55kDa
0 1h 3h 6h 12h 24h 48h 72h
b
MYC-γH2AX colocalization, %
Doxycycline treatment (h)
c
IGH-γH2AX colocalization, %
Doxycycline treatment (h)
d
MYC-IGH translocation
MYC
500bp
0 12 24 48 72 96
Doxycycline treatment (h)
e
MYC-IGH translocations/cells
1x10^-2
5x10^-3
Doxycycline treatment (h)
f
MYC-IGH translocation
Fold Change
Dox
Mirin
NU7026
L67

Fig. 4

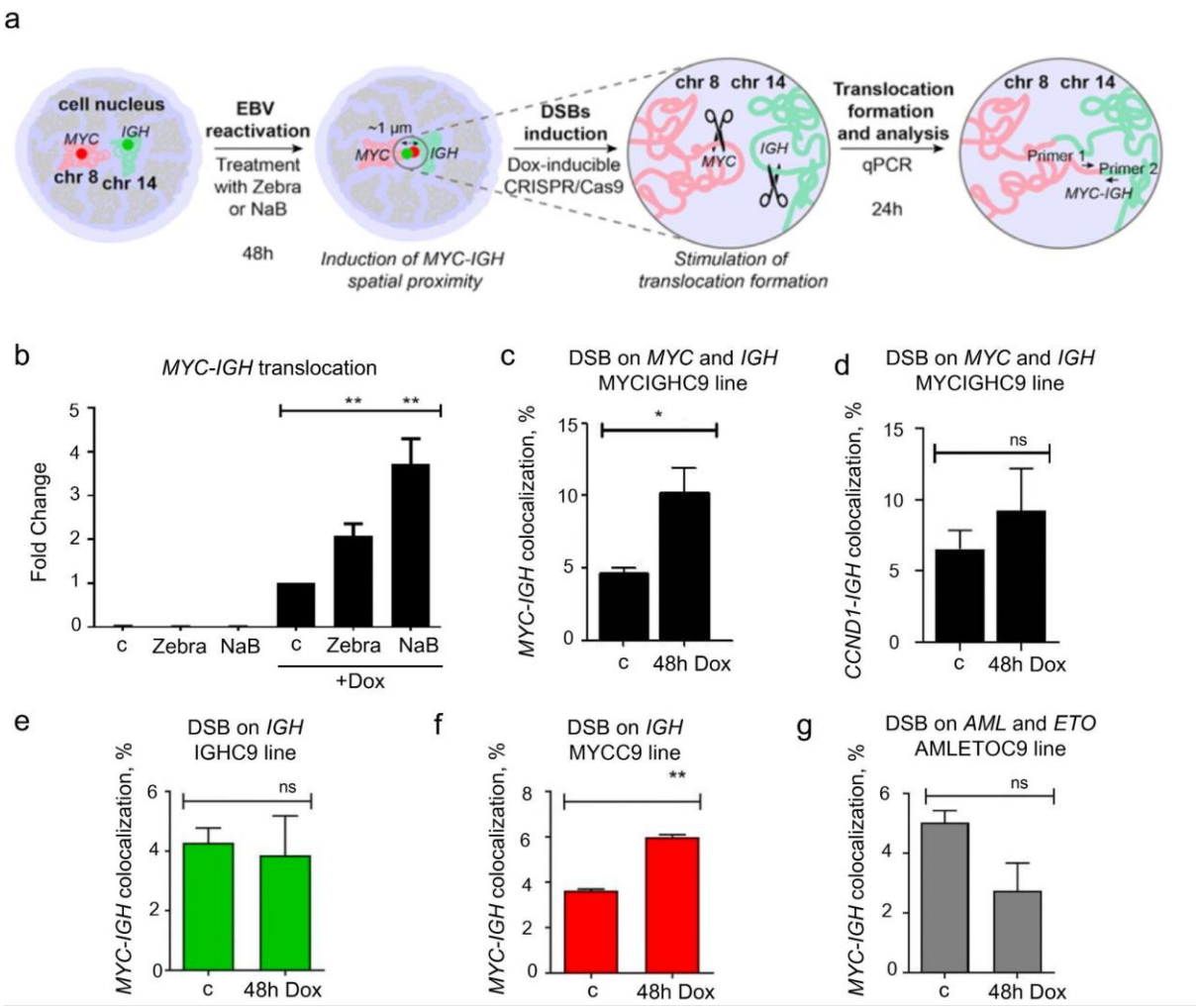
a
cell nucleus
MYC
IGH
chr 8 chr 14
EBV reactivation
Treatment with Zebra or NaB
48h
~1 µm
Induction of MYC-IGH spatial proximity
DSBs induction
Dox-inducible CRISPR/Cas9
Stimulation of translocation formation
Translocation formation and analysis
qPCR
24h
Primer 1
Primer 2
MYC-IGH
b
MYC-IGH translocation
Fold Change
c
Zebra
NaB
+Dox
c
DSB on MYC and IGH
MYCIGHC9 line
MYC-IGH colocalization, %
48h Dox
d
DSB on MYC and IGH
MYCIGHC9 line
CCND1-IGH colocalization, %
ns
e
DSB on IGH
IGHC9 line
f
DSB on IGH
MYCC9 line
g
DSB on AML and ETO
AMLETOC9 line

Fig. 5

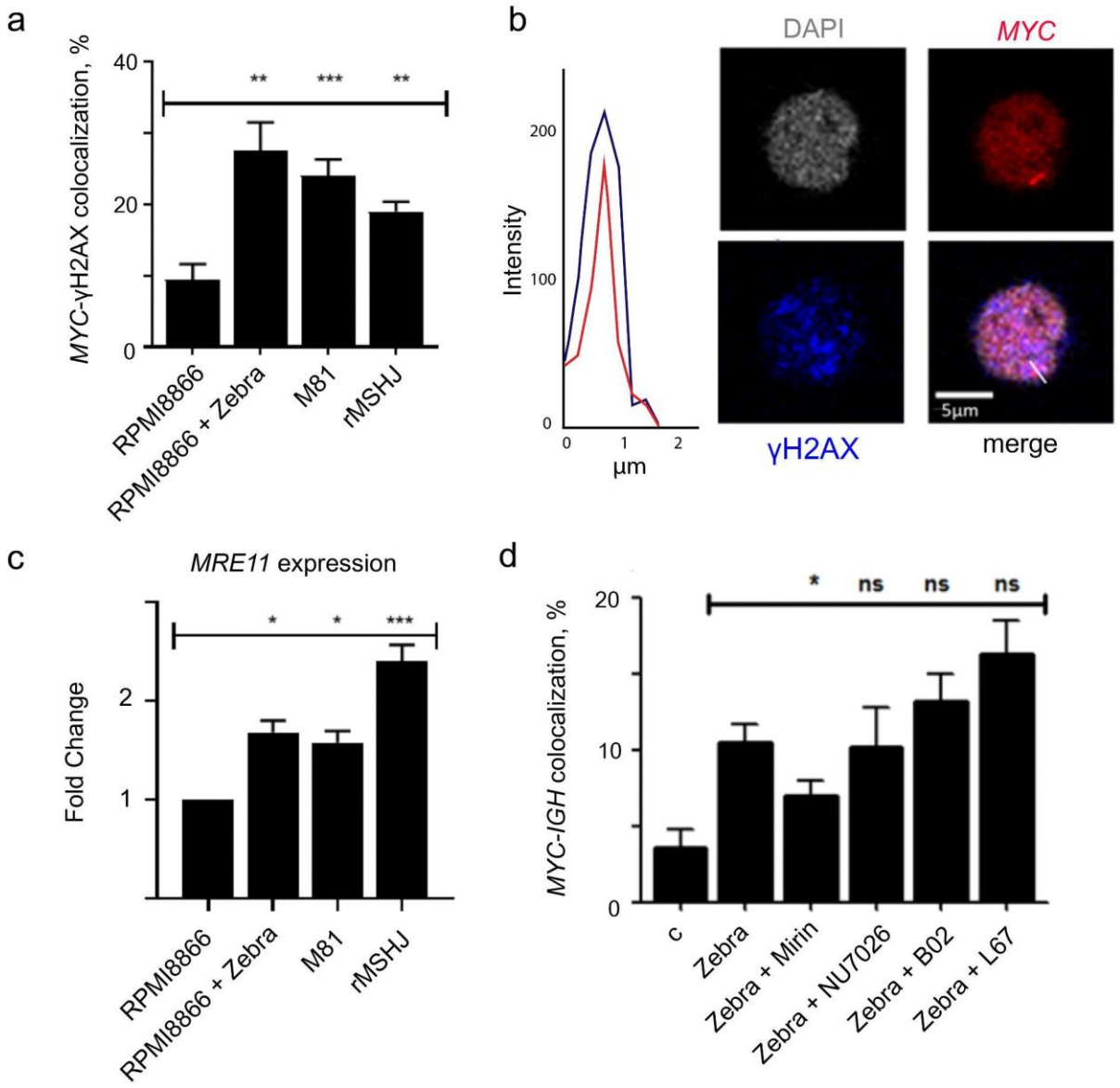
a
MYC-γH2AX colocalization, %
40
20
0
**
***
**
RPMI8866
RPMI8866 + Zebra
M81
rMSHJ
b
DAPI
MYC
Intensity
200
100
0
0
1
2
μm
γH2AX
merge
5μm
c
MRE11 expression
Fold Change
2
1
*
*
***
RPMI8866
RPMI8866 + Zebra
M81
rMSHJ
d
MYC-IGH colocalization, %
20
10
0
*
ns
ns
ns
c
Zebra
Zebra + Mirin
Zebra + NU7026
Zebra + B02
Zebra + L67